

THE PROPERTIES OF HORIZONTAL MAGNETIC ELEMENTS IN QUIET SOLAR INTRANETWORK

Chunlan Jin, Jingxiu Wang and Guiping Zhou

ABSTRACT

Using the data observed by the Solar Optical Telescope/Spectro-Polarimeter aboard the *Hinode* satellite, the horizontal and vertical fields are derived from the wavelength-integrated measures of Zeeman-induced linear and circular polarizations. The quiet intranetwork regions are pervaded by horizontal magnetic elements. We categorize the horizontal intranetwork magnetic elements into two types: one is the non-isolated element which is accompanied by the vertical magnetic elements during its evolution; another is the isolated element which is not accompanied by the vertical magnetic elements. Their properties, such as lifetime, size and magnetic flux density, are studied, and the relationships among various magnetic parameters are investigated.

We identify 446 horizontal intranetwork magnetic elements, among them 87 elements are isolated and 359 are non-isolated. Quantitative measurements reveal that the isolated elements have relatively weaker horizontal magnetic fields, almost equal size, and shorter lifetime comparing with the non-isolated elements. Most non-isolated horizontal intranetwork magnetic elements are identified to associate with the emergence of Ω -shaped flux loops. A few non-isolated elements seem to indicate scenarios of submergence of Ω loops or emergence of U-like loops. There is a positive correlation between the lifetime and the size for both the isolated and non-isolated HIFs. It is also found that there is also positive correlation between the lifetime and the magnetic flux density for non-isolated HIFs, but no correlation for isolated HIFs. Even though the horizontal elements show lower magnetic flux density, they could carry the total magnetic flux in the order of magnitude close to 10^{25} Mx to the solar surface each day.

Subject headings: Sun: evolution — Sun: magnetic fields — Sun: photosphere — techniques: polarimetric

1. INTRODUCTION

It has been known for more than 30 years that the quiet photosphere contains small-scale intranetwork (inter-network, inner-network) (IN) magnetic fields (Smithson 1975; Livingston & Harvey 1975). Most IN magnetic observations have been made at or near disk center using circular-polarization signals that reveal properties of the vertical component of IN fields, such as the intrinsic field strength (e.g., Keller et al. 1994; Lin 1995; López Ariste 2006; Sánchez Almeida 2006), internal structures (e.g., Sánchez Almeida et al. 1996; Lites & Socas-Navarro 2004), and so on. The most prominent are the flux elements of the order of 10^{16} Mx (Wang et al. 1985; Wang et al. 1995; Lin & Rimmele 1999) and their rapid evolution (Shi et al. 1990; Zhang et al. 1998; Berger et al. 1998; Domínguez Cerdeña et al. 2003). The small fluxes and sizes with rapid time changes make the IN magnetic fields provide important contribution to the Sun’s magnetism (Wang et al. 1995; Meunier et al. 1998; Sánchez Almeida & Lites 2000; Lites 2002; Sánchez Almeida 2003; Khomenko et al. 2005; Domínguez Cerdeña et al. 2006a). Moreover, the IN magnetic fields also have important effect on heating solar chromosphere and corona (e.g., Zhang & Zhang 2000; Sánchez Almeida et al. 2004).

However, there is scant information of the IN horizontal magnetic component. By the distinct signature of Stokes Q and U polarization profiles in quiet regions close to the Sun’s disk center based on the observation with the Advanced Stokes Polarimeter, Lites et al. (1996) firstly revealed the isolated, small-scale (typically $1''$ - $2''$ or smaller), short-lived horizontal IN field elements that were abbreviated as HIFs. Meunier et al. (1998) made one-dimension scans across the disk and concluded that the IN magnetic field consisted of relatively stronger vertical features and weaker horizontal component. Harvey et al. (2007) discovered the ubiquitous horizontal component of the solar magnetic field in quiet regions of the photosphere using the observations with different instruments, spectrum lines, and measurements techniques. They found that the horizontal component exhibited wide ranges of spacial and temporal scales: from a few arcseconds up to 15 arcseconds and from several minutes to hours, respectively. The observations from the high spacial resolution of the Solar Optical Telescope (SOT: Tsuneta et al. 2008a; Suematsu et al. 2008; Ichimoto et al. 2008; Shimizu et al. 2008) aboard *Hinode* (Kosugi et al. 2007) and the good polarimetric precision of the Spectro-Polarimeter (SP: Tarbell et al. 2007) provide an access to a new regime of the product of angular resolution and polarimetric precision, and a few papers are concerned with the IN horizontal field. Centeno et al. (2007) study the emergence of magnetic flux at very small spatial scales in the quiet-Sun IN. They find that the horizontal magnetic field appears prior to any significant amount of vertical field. As time goes on, the traces of the horizontal field disappear, while the vertical dipoles are carried by the plasma motions toward the surrounding intergranular lanes. Orozco Suárez et al. (2007a, 2007b) show that IN consists of very inclined, hG fields. Ishikawa et al. (2008) reveal widespread

occurrence of transient, spatially isolated horizontal magnetic fields, and the lateral extent of the horizontal magnetic fields is comparable to the size of the photospheric granules. Lites et al. (2008) reveal that the quiet IN regions are pervaded by horizontal magnetic flux; the horizontal magnetic flux is not associated with network flux. They declare that horizontal magnetic flux is an IN phenomenon. The horizontal fields are somewhat separated spatially from the vertical fields. On average, the horizontal magnetic flux density is apparently larger than the vertical one. Ishikawa & Tsuneta (2009) compared the properties of the transient horizontal magnetic fields in both plage and quiet Sun regions. They show that there are no differences in the distribution and occurrence rate of horizontal fields between the quiet Sun and the plage regions, and there is essentially no preferred orientation for transient horizontal magnetic fields in either region.

In a word, the advance in spatial resolution and sensitivity of SOT/SP observations afforded by *Hinode* presents us with an opportunity to explore the horizontal fields in the quiet IN region, and a new era of studies for horizontal magnetic fields on the quiet Sun is opening.

Here, by the time sequence of solar photospheric observations near the disk center using SOT/SP aboard the *Hinode* satellite, we identify and analyze 87 isolated HIF elements, and 359 non-isolated elements which are 4 times more numerous than that of isolated ones. Their properties, such as the size, lifetime, and magnetic flux density are studied. Furthermore, the relationships among the parameters representing various magnetic properties are investigated. The global contribution of HIFs to the magnetic flux on solar surface is estimated.

In Section 2, we show the observations from SOT/SP aboard the *Hinode* satellite for the selected regions. In Section 3, we describe the technique used to extract horizontal and vertical magnetic fields from wavelength-integrated measures of Zeeman-induced linear polarization and circular polarization. In section 4, we analyze the size, lifetime, and horizontal magnetic flux density, study the relationships among the magnetic parameters, and give the estimation of the contribution of HIFs to the Sun’s magnetic flux. In Section 5, we discuss the topology configuration. In Section 6, we give the summary.

2. OBSERVATIONS

The SP observations in the SOT instruments aboard *Hinode* spacecraft provide the full Stokes spectral signals of two magnetically sensitive FeI lines at 630.15 nm ($g_{eff} = 1.67$) and 630.25 nm ($g_{eff} = 2.5$). The spatial resolution of SP observation is $0''.32$, and the wavelength

sampling is 2.16 pm.

We select 15 time-sequences of fast mode observations close to the disk center, which include 11 quiet regions, 2 ephemeral regions and 2 plage regions (see Table 1). The data in each time-sequence consist of a series of maps with the field of view (FOV) $8''.86 \times 162''.30$. Each map is composed of 30 consecutive positions of spectrograph slit, and the temporal resolution for each map is ~ 2 minutes. In addition, for estimating the magnetic flux carried to the solar surface by the HIFs, we select a quiet solar region of fast mode observation with FOV $118''.89 \times 162''.30$, which was observed at disk center on 2007 May 11 (see Table 1). The region consists of 403 consecutive positions of spectrograph slit.

The scanning steps of the spectrograph slit of fast mode observation are $0''.295$. For the observation of each spectrograph slit, the exposure time is 3.2 seconds. The polarization in solar continuous spectrum of wavelength 630 nm is few according to the results obtained by Stenflo (2005). Therefore, we consider the polarization of continuous spectrum 630 nm from the observation of SP as noise, and derive a noise level of $1.16 \times 10^{-3} I_c$ in Stokes Q and U , and $7.5 \times 10^{-4} I_c$ in Stokes V . Figure 1 shows a randomly selected example of Stokes spectra from the near disk-center time series observation of quiet region.

3. CONVERSION OF POLARIZATION SIGNALS TO MAGNETIC FLUX DENSITY

In this paper, we mostly focus on HIFs, i.e., the horizontal magnetic field elements from the IN fields. In fact, the IN fields have low polarization degree, and mixed and nearly balanced polarity in small scale. Thus, the circular and linear polarization signals from IN fields are very small compared to those from active regions, and extracting the properties of magnetic field from IN is confronted with the measure noise.

Although the inversion codes are robust when applied to the strong Stokes polarization signals from active region, they encounter difficulties in convergence toward and uniqueness of solutions when confronted with noisy profiles (Lites et al. 2008). Therefore, we adopt the procedure of polarization integrated in wavelength of FeI 630.25 nm line to provide the measure of longitudinal and transverse fields (Lites et al. 1999). By this method, we enhance the sensitivity to weak Zeeman polarization in the presence of measurement noise, and avoid the problems of convergence and non-uniqueness that result from the inversion of noisy profiles.

The wavelength-integrated circular polarization V_{tot} from Stokes $V(\lambda)$ is defined as

$$V_{tot} = \text{sign}(V_{blue}) \frac{|\int_{\lambda_b}^{\lambda_0} V(\lambda) d\lambda| + |\int_{\lambda_0}^{\lambda_r} V(\lambda) d\lambda|}{I_c \int_{\lambda_b}^{\lambda_r} d\lambda} \quad (1)$$

where $\text{sign}(V_{blue})$ means the sign of the blue peak of the Stokes V profile, λ_0 describes the wavelength of line center (i.e., the wavelength corresponding to the minimum value of $I(\lambda)$), λ_r and λ_b show the integrated limit of the red and the blue over the line FeI 630.25 nm, with $\lambda_r = \lambda_0 + 35$ pm and $\lambda_b = \lambda_0 - 35$ pm, I_c means the continuum intensity. Furthermore, we also define the linear polarization L_{tot} with the same method,

$$L_{tot} = \frac{\int_{\lambda_b}^{\lambda_r} [Q^2(\lambda) + U^2(\lambda)]^{1/2} d\lambda}{I_c \int_{\lambda_b}^{\lambda_r} d\lambda} \quad (2)$$

Where $Q(\lambda)$ and $U(\lambda)$ is the intensity of Stokes Q and U in wavelength λ .

Jefferies, Lites, & Skumanich (1989) demonstrated that, in the weak field limit

$$fB^2 \sin^2 \gamma \propto (\int_0^\infty [Q^2(\lambda) + U^2(\lambda)]^{1/2} d\lambda) / D \quad (3)$$

$$fB \cos \gamma \propto (\int_0^\infty |V(\lambda)| d\lambda) / D \quad (4)$$

Where f is the filling factor, B is the magnetic field strength, γ is the inclination angle corresponding to the line of sight (LOS), and $D = I_c - I(\lambda = 0)$ is the line depth at line center. Therefore, Lites et al. (1999) used inversions of the stronger polarization signals in quiet solar spectropolarimetric maps to calibrate circular polarization into longitudinal fields. Following that work, we inverted the pixels with stronger linear and circular polarization signals primarily from the network flux elements to determine the calibration constants relating linear polarization to transverse fields and circular polarization to longitudinal fields.

Martínez González et al. (2006) demonstrate the pair of FeI lines in low magnetic flux quiet Sun regions is not capable of distinguishing between the intrinsic magnetic field and the filling factor. Therefore, the magnetic flux density is a more appropriate quantity to describe the equivalent, spatially resolved vector magnetic fields, i.e., the longitudinal and the transverse components, B_{app}^L and B_{app}^T . The longitudinal component B_{app}^L may be thought of as the magnitude of the LOS component of a spatially resolved magnetic field that produces the observed circular polarization signal, while the transverse component B_{app}^T is perpendicular to the LOS that would produce the observed linear polarization signal. Figure 2 shows the relationships of measured V_{tot} as a function of the longitudinal flux density B_{app}^L

inferred from the inversion, $f|B|\cos(\gamma)$, and measured L_{tot} as a function of the transverse flux density B_{app}^T derived from the inversion, $f^{1/2}|B|\sin(\gamma)$. We have used the inversion code developed by the Japanese *Hinode* group based on the assumption of Milne-Eddington atmosphere (T. Yokoyama 2009, in preparation).

4. PROPERTIES OF HORIZONTAL INTRANETWORK MAGNETIC ELEMENTS

4.1. Size, Lifetime, And Horizontal Magnetic Flux Density

For each horizontal magnetic element, we begin to track it when its linear polarization signal is obviously larger than the noise level, and we think it disappears when its linear polarization is difficult to distinguish from the noise. We selected 446 independent HIFs by identifying and tracking each of them from birth to death. They cover almost all the prominent HIFs seen from the 15 time-sequence of the quiet sun horizontal field measurements. We quantitatively measure the lifetime, size and average horizontal magnetic flux density, respectively, for each horizontal magnetic element.

Lites et al. (2008) point out that the horizontal fields do not simply arise from convective buffeting of strong, nearly vertical fields. Symmetric Stokes Q and U signatures are not accompanying strong antisymmetric Stokes V profiles (Lites et al. 1996). Moreover, only 16% of the area within the 3σ horizontal fields contours overlaps with area within the contours of vertical fields (Lites et al. 2008). Therefore, we categorized the HIFs into two classes. If the circular polarization signals tempo-spatially accompanying the HIFs are always less than the noise level of circular polarization during the evolution of HIFs, then we would define these horizontal elements as isolated HIFs. To the contrary, if there are clear circular polarization signals above the noise tempo-spatially accompanying the HIFs, we would called them as non-isolated HIFs. Thus, it is found that there are 87 isolated HIFs and 359 non-isolated HIFs. A case of evolution non-isolated HIFs is displayed in the top two panels of Fig. 3. From this figure, we can find that there are always two vertical magnetic elements with opposite polarities on both sides of the HIF (denoted by dotted lines) during its evolution, and the two vertical magnetic elements still exist after disappearance of the HIF. Moreover, the two vertical magnetic elements (denoted by arrows at 07:56 UT) with opposite polarities separate. An example of isolated HIFs (displayed by dotted lines) is shown in the lower two panels of Fig. 3. For the isolated HIF, there are no vertical magnetic elements during its evolution, even after its disappearance.

Because the spatial size and average horizontal magnetic flux density are changing dur-

ing the process of HIFs' evolution, we define the largest size during the evolution as the spatial size of HIFs and the largest horizontal magnetic flux density during the evolution as the horizontal magnetic flux density of HIFs. Furthermore, we define the lifetime of HIF according to the number of maps of the appearance of HIF. That is to say, in the maps of time series, if there is only one map which shows the HIF, we will define the lifetime of the HIF as 2 minutes, though it may not be exactly true. The properties of HIFs are shown in Table 2.

Figure 4 shows the histogram of the lifetime of HIFs. The dotted line shows the histogram of lifetime for isolated HIFs, the dash-dot-dot line for non-isolated HIFs, and the solid line for all HIFs. From the figure, we can find that the lifetime of these isolated HIFs ranges from 2 minutes to 14 minutes with a peak distribution at 4 minutes, while the lifetimes of these non-isolated HIFs range from 2 minutes to 14 minutes with a peak distribution at 6 minutes. The mean lifetime is 4.3 minutes for isolated HIFs and 5.9 minutes for non-isolated HIFs, respectively. On average, the lifetime of isolated HIFs is shorter than that of non-isolated HIFs.

Figure 5 shows the histograms of the size of all HIFs (displayed by the solid line), the isolated HIFs (showed by dotted line) and the non-isolated HIFs (denoted by dash-dot-dot line), respectively. Because the shapes of these horizontal magnetic elements are irregular, the size of horizontal magnetic element is defined as follows: Let A be the area of horizontal magnetic element, and an effective size is $D = 2(A/\pi)^{1/2}$. The size of these isolated HIFs ranges from $0''.62$ to $1''.48$ with a peak distribution at about $1''.00$, while the size of these non-isolated HIFs ranges from $0''.72$ to $2''.04$ with a peak distribution at about $1''.15$. The mean size is $1''.07$ for isolated HIFs and $1''.14$ for non-isolated HIFs. On average, the size of isolated HIFs is less than that of non-isolated HIFs.

Figure 6 shows the histogram of the horizontal magnetic flux density of HIFs. The horizontal magnetic flux density of these isolated HIFs range from 247 Mx cm^{-2} to 304 Mx cm^{-2} with a peak distribution around 257 Mx cm^{-2} , while the horizontal magnetic flux density of these non-isolated HIFs range from 248 Mx cm^{-2} to 330 Mx cm^{-2} with a peak distribution at about 267 Mx cm^{-2} . The mean horizontal magnetic flux density is 264 Mx cm^{-2} for isolated HIFs and 273 Mx cm^{-2} for non-isolated HIFs. The horizontal magnetic flux density of isolated HIFs is averagely smaller than that of non-isolated HIFs.

In order to test whether the difference of properties between isolated HIFs and non-isolated HIFs is remarkable, we make the statistical test. Here, we give the detail description of the statistical test. Taking an example of the difference between the average sizes of isolated HIFs and non-isolated HIFs. The steps are following: (1) we assume H_0 : the average size of isolated HIFs is equal to that of non-isolated HIFs; (2) we confirm the distribution

of the statistical variable. In general, when the number of sample is larger than 30, the sample is considered to a large sample. For a large sample, a normal distribution for the average value of the sample can be considered according to the central limit theorems; (3) a significance level α is given. Here, the value α is assumed to be 0.1% by us; (4) the confidence limit is checked according to the table of normal distribution. $\int_{-k_{\frac{\alpha}{2}}}^{k_{\frac{\alpha}{2}}} \frac{1}{\sqrt{2\pi}} e^{-\frac{v^2}{2}} dv = 1 - \alpha$. We can obtain the $k_{0.0005} = 3.29$ by checking the table of normal distribution; (5) the statistical variable is computed by the formula: $u = \frac{\bar{x}_1 - \bar{x}_2}{\sqrt{\frac{\sigma_1^2}{n_1} + \frac{\sigma_2^2}{n_2}}}$, where σ_1^2 is the sample variance of the non-isolated HIFs, n_1 is number of non-isolated HIFs, σ_2^2 is the sample variance of the isolated HIFs, and n_2 is number of isolated HIFs. Here, \bar{x}_1 is the average size of non-isolated HIFs, and \bar{x}_2 is the average size of isolated HIFs. We compute that the value of statistical variable is 3.05; (6) the statistical verdict is given: when $|u| < k_{\frac{\alpha}{2}}$, the assumption of H_0 is right; when $|u| \geq k_{\frac{\alpha}{2}}$, the assumption of H_0 is wrong. Because the statistical variable u is less than $k_{\frac{\alpha}{2}}$ by our computation, the assumption of the same size of isolated HIFs and non-isolated HIFs is right. That is to say, the average size of isolated HIFs is equal to that of non-isolated HIFs with a confidence level of 99.9%.

Following above steps, we also test the distinctions of average lifetime and average horizontal magnetic flux density between isolated HIFs and non-isolated HIFs, and we find that the average lifetime and average horizontal magnetic flux density of isolated HIFs are less than those of non-isolated HIFs with a confidence level of 99.9%. Although the distinction between the isolated and non-isolated HIFs is clear in a sense of statistics, it is not clear whether or not the two kinds of HIFs have different origins and if they represent intrinsically different types of magnetic fields.

4.2. Relationships Among The Magnetic Parameters

The correlation between the horizontal magnetic flux density and lifetime of HIFs is studied. In order to show the relationship clearly, we divide the horizontal magnetic flux density into 7 bins for non-isolated HIFs, and 5 bins for isolated HIFs according to the lifetime (range from 2 minutes to 14 minutes for non-isolated HIFs, and from 2 minutes to 10 minutes for isolated HIFs). Moreover, we compute the mean horizontal magnetic flux density in each bin. The correlation is shown in Fig. 7. From the figure, we find that there is a positive correlation between them for non-isolated HIFs, and the correlation coefficient is 0.917, well above the confidence level of 99.9%. However, we find that there is no relationship between them for isolated HIFs due to a small correlation coefficient of 0.053.

In addition, by the same way, we also analyze the relationship between the lifetime and

the corresponding size of HIFs, just as shown in Fig. 8. Our statistics display that there is a positive correlation between them for both non-isolated HIFs and isolated HIFs, and their correlation coefficients are 0.924 and 0.986, respectively, both of them well above the confidence level of 99.9%.

4.3. Contribution of HIFs to The Sun’s Magnetic Flux

B_{app}^T approximately describes the horizontal field strength if the HIFs were actually completely resolved in our observation. Furthermore, there are two methods to obtain the horizontal magnetic field of each pixel. One is the horizontal magnetic flux density by allowing for variable filling fraction in the inversion. Another is the horizontal field strength by assuming the resolved HIFs in the observation and unit filling fraction in the inversion. The horizontal magnetic fields obtained by the two methods yield very nearly the same average value (Lites et al. 1996).

Considering the evolution of HIFs, we estimate the magnetic flux carried to the solar surface by these horizontal elements by assuming the variable filling fraction in the inversion. The magnetic flux in one HIFs, $\psi \approx B_{app}^T D d$ is about 2.2×10^{17} Mx for horizontal magnetic flux density B_{app}^T of 271 Mx cm^{-2} , the size D of $1''.13$ (820 km) and assuming a vertical extension in the atmosphere of 100 km (comparable to the photospheric scale height, so that the flux elements are actually observable). In figure 9, we find that the quiet IN regions are pervaded by horizontal magnetic elements, and the mean number density of HIFs is ~ 0.015 per arcsec^2 . Given that the mean lifetime of HIFs is ~ 5.6 minutes, we can obtain the rate of 4.46×10^{-5} HIFs $\text{arcsec}^{-2}\text{s}^{-1}$. Therefore, almost 9.82×10^{24} Mx over the solar surface per day, or 3.94×10^{28} Mx per 11 year sunspot cycle is carried to solar surface by the HIFs. The flux emergence rate is similar to the estimation of the HIFs by Lites et al. (1996) and the IN vertical flux emergence by Wang et al. (1995). Moreover, the horizontal fields also contribute to the "hidden" turbulent flux suggested by studies involving Hanle effect depolarization of scattered radiation (Lites et al. 2008). Tsuneta et al. (2008b) point that the polar region is also covered with ubiquitous horizontal fields. Thus, even if we exclude 30% of the solar surface for network and active region, this is still more than the accepted value of the total flux though to emerge in bipolar sunspot regions during an entire solar cycle, of order 10^{25} Mx (Harvey 1993). The result agrees with the conclusion drawn by Domínguez Cerdeña (2006b) who find that the quiet Sun photosphere has far more unsigned magnetic flux than the active regions and the network together. Indeed, the solar IN fields contribute the most of the solar magnetic flux in the solar surface.

5. DISCUSSION OF THE TOPOLOGY CONFIGURATION

With regard to the magnetic flux shown in the photosphere, there are two possible topology configurations for the magnetic loop: one is the Ω loop for traditional emerging flux region (Bruzek 1967; Zwaan 1978), and another is U loop, suggested for IN magnetic elements by Spruit et al. (1987). For the both types of topology, the horizontal fields are associated with the vertical fields, and the footpoints of magnetic loop stand at each side of the region of linear polarization signals. However, the detailed scenario of the vertical and horizontal field evolution for the non-isolated HIFs would tell which topology is truly correct. If the vertical fields are separating and growing during the HIF's appearance, then we are quiet sure the HIF represents an emerging Ω flux loops. On the other hand, if the HIF appeared during the shrinkage and reduction of vertical fields, we should expect an emerging U loop. The submergence of an Ω would show the same scenario as U loop emergence, but the horizontal field orientation would be opposite to the later case.

Keeping the above discussion in mind we find the magnetic topology configurations for the Ω loop that are shown in the top two panels of Fig. 10. At 14:59 UT, the horizontal field shows up in the photosphere as a non-isolated HIF. At 15:07 UT, the horizontal element disappears while the corresponding vertical magnetic fields (denoted by circles) with opposite polarities separate. In our studies, some non-isolated HIFs only display one footpoint of in a side of horizontal fields. A similar example is shown in the middle two panels of Fig. 10. From 03:15 UT to 03:23 UT, the horizontal magnetic element is being accompanied by the positive vertical magnetic element. This is not conflicting with the traditional picture of flux emergence. Wang and Shi (1993) demonstrated that when an emerging flux region appeared in an area of magnetic flux with one dominant polarity, the subsurface magnetic reconnection could hide one polarity footpoint shown up in the photosphere.

However, under the conditions of spatial resolution of $0''.32$ and temporal resolution of ~ 2 minutes, we can always not distinguish if the observed magnetic configurations are Ω loop or U loop, according to the evolutions of horizontal and vertical magnetic elements. A case is shown in the bottom two panels of Fig. 10. From 11:54 UT to 11:56 UT, two negative vertical magnetic elements and a positive vertical magnetic element are going with the horizontal magnetic element (denoted by dotted lines). At 11:58 UT, the horizontal magnetic element suddenly disappears, and the vertical magnetic flux shows mutual flux disappearance, i.e., flux cancellation (Live et al. 1985; Martin et al. 1985). During the flux cancellation, a negative vertical magnetic element almost vanishes. Without resolving the 180 degree ambiguity of field azimuth in the observed vector fields, we have difficulty to finally determine if the observed HIF evolution represents a submergence of an Ω loop or the emergence of an Ω loop.

In addition, the distinction in properties between isolated and non-isolated HIFs seem to offer a rather consistent picture about the HIFs. The non-isolated HIFs are likely to be the stronger horizontal field threads which have already overstepped the criteria of buoyancy instability; thus they emerge in the form of Ω loops, showing up the non-isolated HIFs. The isolated HIFs come from weaker horizontal field threads beneath the photosphere. They appear as the isolated HIFs by pumping force from local convection. Therefore it is reasonable to propose that beneath the photosphere there are sea of horizontal magnetic threads which manifest as HIFs in the photosphere either by buoyancy instability or the pumping force of the local convection.

6. SUMMARY

Using the data observed by the SOT/SP aboard the *Hinode*, the properties of HIFs, such as the size, lifetime, and horizontal magnetic flux density of HIFs are studied, and the relationships among these properties of HIFs are investigated.

We select 446 HIFs by identifying and tracking each of them from birth to death, and find that there are 87 isolated HIFs and 359 non-isolated HIFs which is more numerous than that the former by a factor of 4. We find that the lifetime of HIFs ranges from 2 minutes to 14 minutes with a peak lifetime of 6 minutes, and the result is obviously different from the conclusion drawn by Harvey et al. (2007) for seething horizontal magnetic fields in the quiet solar photosphere. A wide range of temporal scales from several minutes to hours was reported for their seething fields. More studies are needed to clarify the discrepancy, and particularly if different authors are dealing with different species of horizontal fields. The mean lifetime of HIFs is 5.6 minutes, and the result confirms the conclusion drawn by Lites et al. (1996) who find that the horizontal elements are short-lived, typically lasting ~ 5 minutes. On average, the lifetime of isolated HIFs is shorter than that of non-isolated HIFs. The range of size is from $0''.62$ to $1''.48$ for isolated HIFs with a peak distribution at about $1''.00$, and from $0''.72$ to $2''.04$ for non-isolated HIFs with a peak distribution at about $1''.15$. The size of HIFs obtained by us agrees with the size of horizontal magnetic flux structures presented by Lites et al. (1996) who firstly reveal the small-scale (typically $1''$ - $2''$ or smaller) horizontal elements. We find that the size of isolated HIFs is averagely equal to that of non-isolated HIFs in a sense of statistics. However, the horizontal magnetic flux density of isolated HIFs is less than that of non-isolated HIFs on average.

There is a positive correlation between the lifetime and the size for both the isolated and non-isolated HIFs. It is also found that there is also positive correlation between the lifetime and the magnetic flux density for non-isolated HIFs, but no correlation for isolated

HIFs. Even though the horizontal elements show lower magnetic flux density, they could carry the total magnetic flux in the order of magnitude close to 10^{25} Mx to the solar surface each day.

In fact, the term "horizontal magnetic elements" in this research is not strict in a way. Because these regions selected by us are not severely at disk center, the linear polarization also includes the fractional information of vertical fields. Thusly, the horizontal and vertical magnetic fields in the research are contained each other in some sense. However, part of the 15 regions are very close to the disk center, and the largest offset of the regions from disk center is approximately 200 arcseconds. Considering the rather large error possibly resulted from de-projection, we did not make the correction of projection. The observed transverse fields are dominantly contributed by the horizontal field component. The properties of HIFs described in this study approximately represent the true nature of the quiet Sun's horizontal field.

The authors are grateful to the *Hinode* team for providing the data. *Hinode* is a Japanese mission developed and launched by ISAS/JAXA, with NAOJ as a domestic partner and NASA and STFC (UK) as international partners. The authors are also thankful to Jingyuan Liu from Beijing Normal University. It is operated by these agencies in cooperation with ESA and NSC (Norway). This work is supported by the National Natural Science Foundations of China (10703007, 10873020, G10573025, 40674081, 10603008, 40890161, and 10733020), the Chinese Academy of Sciences Project KJCX2-YW-T04, and the National Basic Research Program of China (G2006CB806303).

REFERENCES

- Berger Thomas E., Lofdahl Mats G., Shine Richard S., et al. 1998, ApJ, 495, 973
- Bruzek, A. 1967, Sol. Phys., 2, 451
- Centeno, R., Socas-Navarro, H., Lites, B., et al. 2007, ApJ, 666, L137
- Domínguez Cerdeña, I., Sánchez Almeida, J., Kneer, F. 2003, A&A, 407, 741
- Domínguez Cerdeña, I., Sánchez Almeida, J., Kneer, F. 2006a, ApJ, 636, 496
- Domínguez Cerdeña, I., Sánchez Almeida, J., Kneer, F. 2006b, ASPC, 358, 48
- Harvey, J. W., Branston, D., Henney, C. J., et al. 2007, ApJ, 659, 177L

- Harvey, K. 1993, Ph.D. thesis, University Utrecht
- Ichimoto, K., Lites, B., Elmore, D., et al. 2008, *Sol. Phys.*, 249, 233
- Ishikawa, R., Tsuneta, S., Ichimoto, K., et al. 2008, *A&A*, 481, 25
- Ishikawa, R., & Tsuneta, S. 2009, *A&A*, in press
- Jefferies, J., Lites, B. W., & Skumanich, A. 1989, *ApJ*, 343, 920
- Keller, C. U., Deubner, F. L., Egger, U., et al. 1994, *A&A*, 286, 626
- Khomenko, E. V., Martínez González, M. J., Collados, M., et al. 2005, *A&A*, 436, 27
- Kosugi, T., Matsuzaki, K., Sakao, T., et al. 2007, *Sol. Phys.*, 243, 3
- Lin, H. S. 1995, *ApJ*, 446, 421
- Lin, H. S., & Rimmele, Thomas 1999, *ApJ*, 514, 448
- Livi, S. H. B., Wang, J., & Martin, S. F. 1985, *AuJPh*, 38, 855
- Livingston, W. C., & Harvey, J. 1975, *BAAS*, 7, 346
- Lites, B. W. 2002, *ApJ*, 573, 431
- Lites, B. W., Kubo, M., Socas-Navarro, H., et al. 2008, *ApJ*, 672, 1237
- Lites, B. W., Leka, K. D., Skumanich, A., et al. 1996, *ApJ*, 460, 1019
- Lites, B. W., Rutten, R. J., & Berger, T. E. 1999, *ApJ*, 517, 1013
- Lites, B. W., & Socas-Navarro, H. 2004, *ApJ*, 613, 600
- López Ariste, A., Tomczyk, S., & Casini, R. 2006, *A&A*, 454, 663
- Martínez González, M. J., Collados, M. & Ruiz Cobo, B. 2006, *A&A*, 456, 1159
- Martin, S. F., Livi, S. H. B., & Wang, J. 1985, *AuJPh*, 38, 929
- Meunier, N., Solanki, S. K., & Livingston, W. C. 1998, *A&A*, 331, 771
- Orozco Suárez, D., Bellot Rubio, L. R., Del Toro Iniesta, J. C., et al. 2007a, *ApJ*, 670, L61
- Orozco Suárez, D., Bellot Rubio, L. R., Del Toro Iniesta, J. C., et al. 2007b, *PASJ*, 59, 837
- Shi, Z. X., Wang, J. X., Liu, J. Q., et al., 1990, *ChA&A*, 14, 325

- Shimizu, T., Nagata, S., Tsuneta, S., et al. 2008, *Sol. Phys.*, 249, 221
- Sánchez Almeida, J. 2003, *AIPC*, 679, 293
- Sánchez Almeida, J. 2006, *A&A*, 450, 1199
- Sánchez Almeida, J. Landi degl’Innocenti, E., Martinez Pillet, V., et al. 1996, *ApJ*, 466, 537
- Sánchez Almeida, J. & Lites, B. W., 2000, *ApJ*, 532, 1215
- Sánchez Almeida, J., Márquez, I., Bonet, J. A., et al. 2004, *ApJ*, 609, L91
- Smithson, R. C. 1975, *BAAS*, 7, 346
- Spruit, H. C., Title, A. M., & Van Ballegooijen A. A. 1987, *Sol. Phys.*, 110, 115
- Stenflo, J. O. 2005, *A&A*, 429, 713
- Suematsu, Y., Tsuneta, S., Ichimoto, K., et al. 2008, *Sol. Phys.*, 249, 197
- Tarbell, T. D., Lites, B. W., Shine, R. A., et al. 2007, *AAS*, 210, 9401
- Tsuneta, S., Ichimoto, K., Katsukawa, Y., et al., 2008a, *Sol. Phys.*, 249, 167
- Tsuneta, S., Ichimoto, K., Katsukawa, Y., et al., 2008b, *ApJ*, 688, 1374
- Wang, J. X., & Shi, Z. X. 1993, *Sol. Phys.*, 143, 119
- Wang, J. X., Wang, H. M., Tang, Frances, et al. 1995, *Sol. Phys.*, 160, 277
- Wang, J. X., Zirin, H., & Shi, Z. 1985, *Sol. Phys.*, 98, 241
- Yokoyama, T. 2009, in preparation
- Zhang, H. Q., & Zhang, M. 2000, *Sol. Phys.*, 196, 269
- Zhang, J., Lin, G. H., Wang, J. X., et al. 1998, *Sol. Phys.*, 178, 245
- Zwaan C. 1978, *Sol. Phys.*, 60, 213

Table 1: The used data.

	Date	Time Range	Location	Property
1	April 7, 2007	11:05-13:59 UT	(-5", -170")	ephemeral region
2	April 12, 2007	11:06-11:58 UT	(-6", 0")	quiet region
3	April 13, 2007	03:07-04:05 UT	(-155", -169")	plage region
4	April 13, 2007	04:36-05:42 UT	(-155", -169")	plage region
5	April 13, 2007	13:05-13:40 UT	(-98", 0")	quiet region
6	April 13, 2007	15:05-15:45 UT	(-80", 0")	quiet region
7	June 1, 2007	14:13-15:20 UT	(-31", -200")	quiet region
8	June 1, 2007	15:52-16:58 UT	(-31", -200")	quiet region
9	June 2, 2007	11:48-12:40 UT	(0", -200")	quiet region
10	June 2, 2007	14:51-15:57 UT	(0", -200")	quiet region
11	June 2, 2007	16:29-17:35 UT	(0", -200")	quiet region
12	June 3, 2007	13:50-14:56 UT	(0", -200")	quiet region
13	June 3, 2007	15:28-16:34 UT	(0", -200")	quiet region
14	June 4, 2007	02:58-04:04 UT	(0", 200")	quiet region
15	November 13, 2007	07:06-10:00 UT	(-140", -50")	ephemeral region
16	May 11, 2007	01:05-01:35 UT	(-14", 0")	quiet region

Table 2: The properties of HIFs.

Properties	mean	deviation	minimum	maximum
lifetime _{iso} (min)	4.3	1.9	2.0	10.0
lifetime _{non-iso} (min)	5.9	2.5	2.0	14.0
lifetime _{all} (min)	5.6	2.4	2.0	14.0
B _{iso} (Mx cm ⁻²)	264	11	247	304
B _{non-iso} (Mx cm ⁻²)	273	15	248	330
B _{all} (Mx cm ⁻²)	271	15	247	330
size _{iso} (arcsec)	1.07	0.19	0.62	1.48
size _{non-iso} (arcsec)	1.14	0.20	0.72	2.04
size _{all} (arcsec)	1.13	0.20	0.62	2.04
number		446		

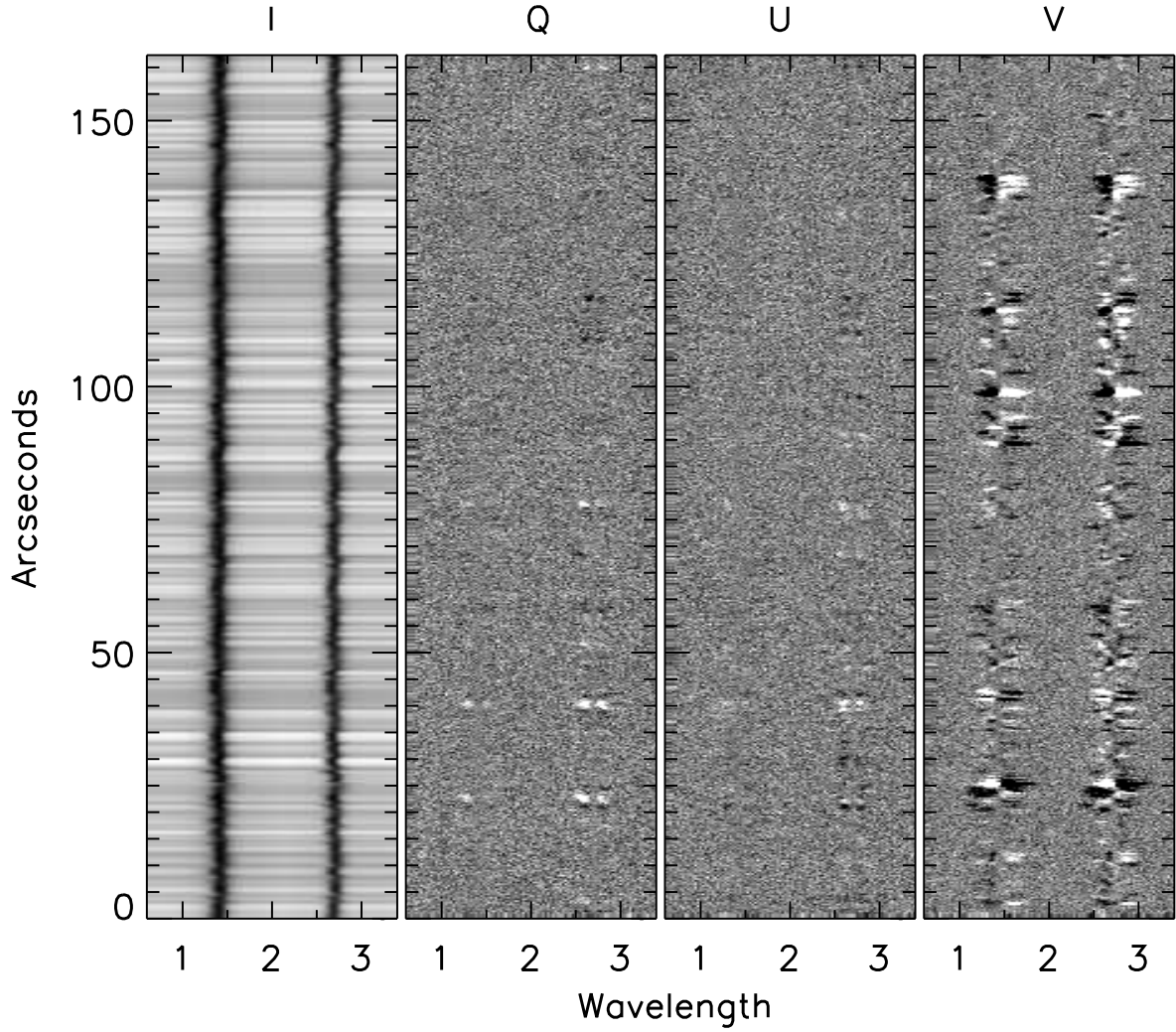


Fig. 1.— A random example of Stokes I , Q , U , V profiles. These spectra were obtained near disk center at 11:08 UT on 2007 April 12 with an integration for 3.2s. The gray scale for Q , U , V saturates at $\pm 0.003 I_c$. There are 112 spectral samples of 2.16 pm.

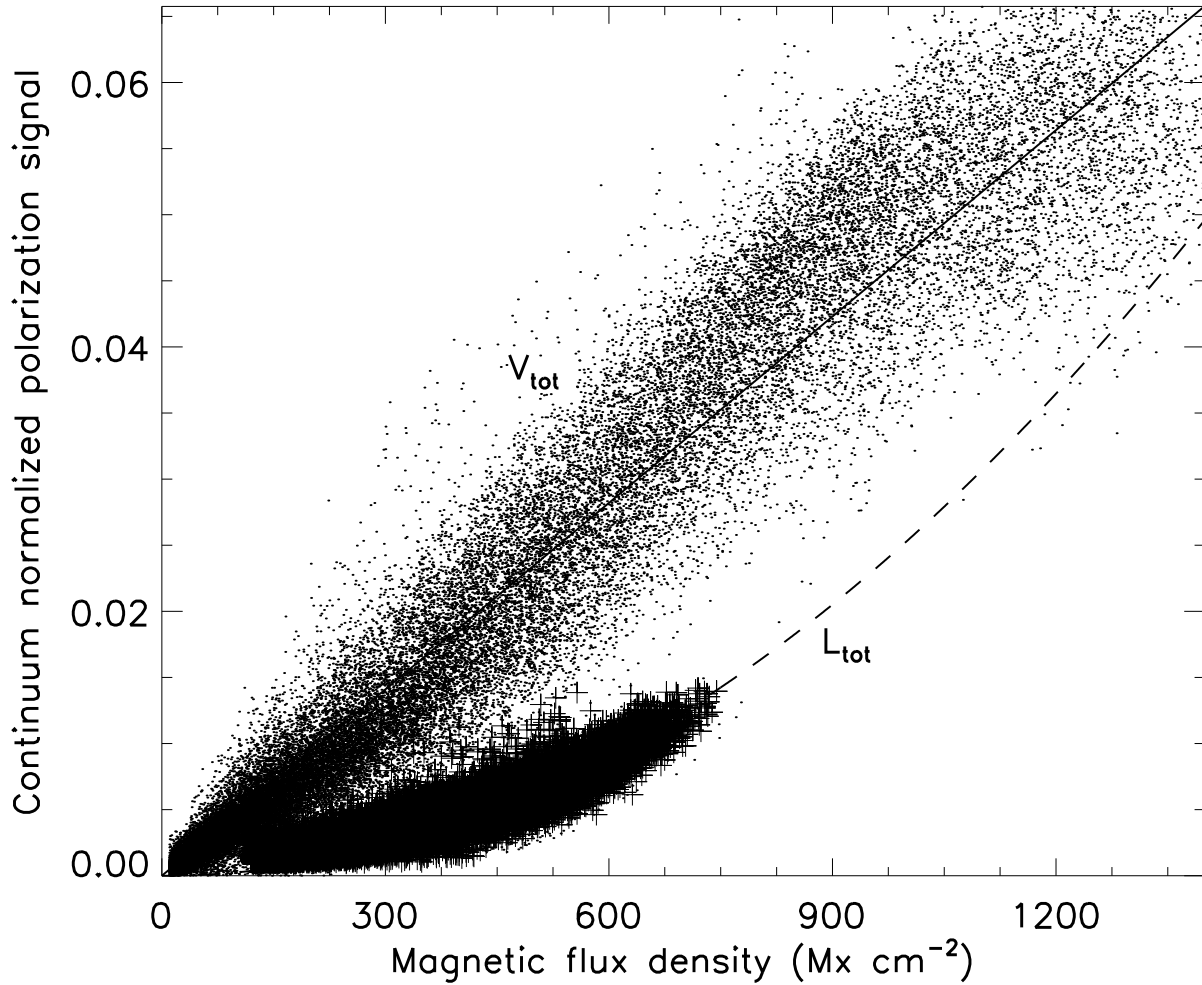


Fig. 2.— Calibration curves converting wavelength integral measurements of circular polarization V_{tot} (solid line) and linear polarization L_{tot} (dashed line) to magnetic flux density. The period and plus signs mean the inversion of the stronger flux region, where both the linear polarization and circular polarization are greater than 3 times noise level.

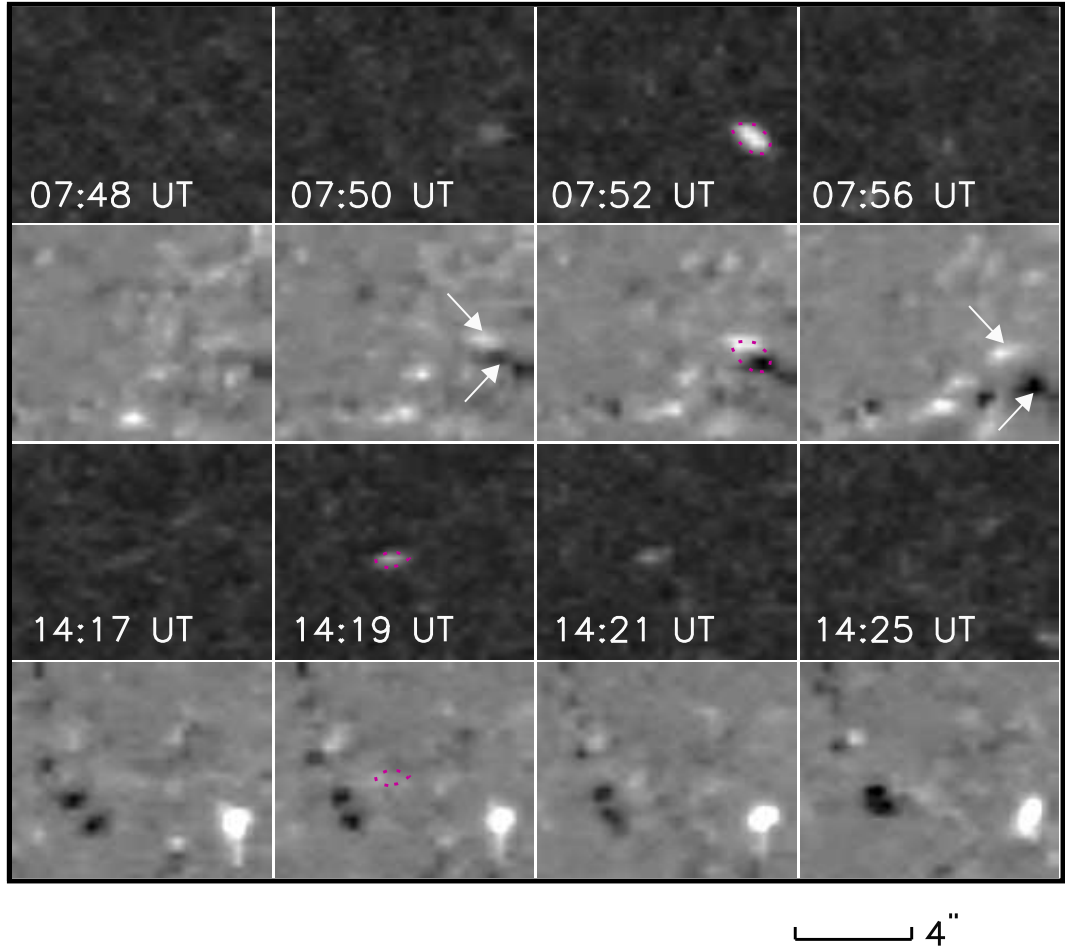


Fig. 3.— Example of isolated and non-isolated HIFs. The first line shows the evolution of non-isolated HIFs observed on 2007 November 13, and the second line is the corresponding evolution of vertical field. The third line describes the evolution of isolated HIFs observed on 2007 June 1, and the corresponding evolution of vertical field is shown in the fourth line. The bar in the low right corner represents the scale of 4''.

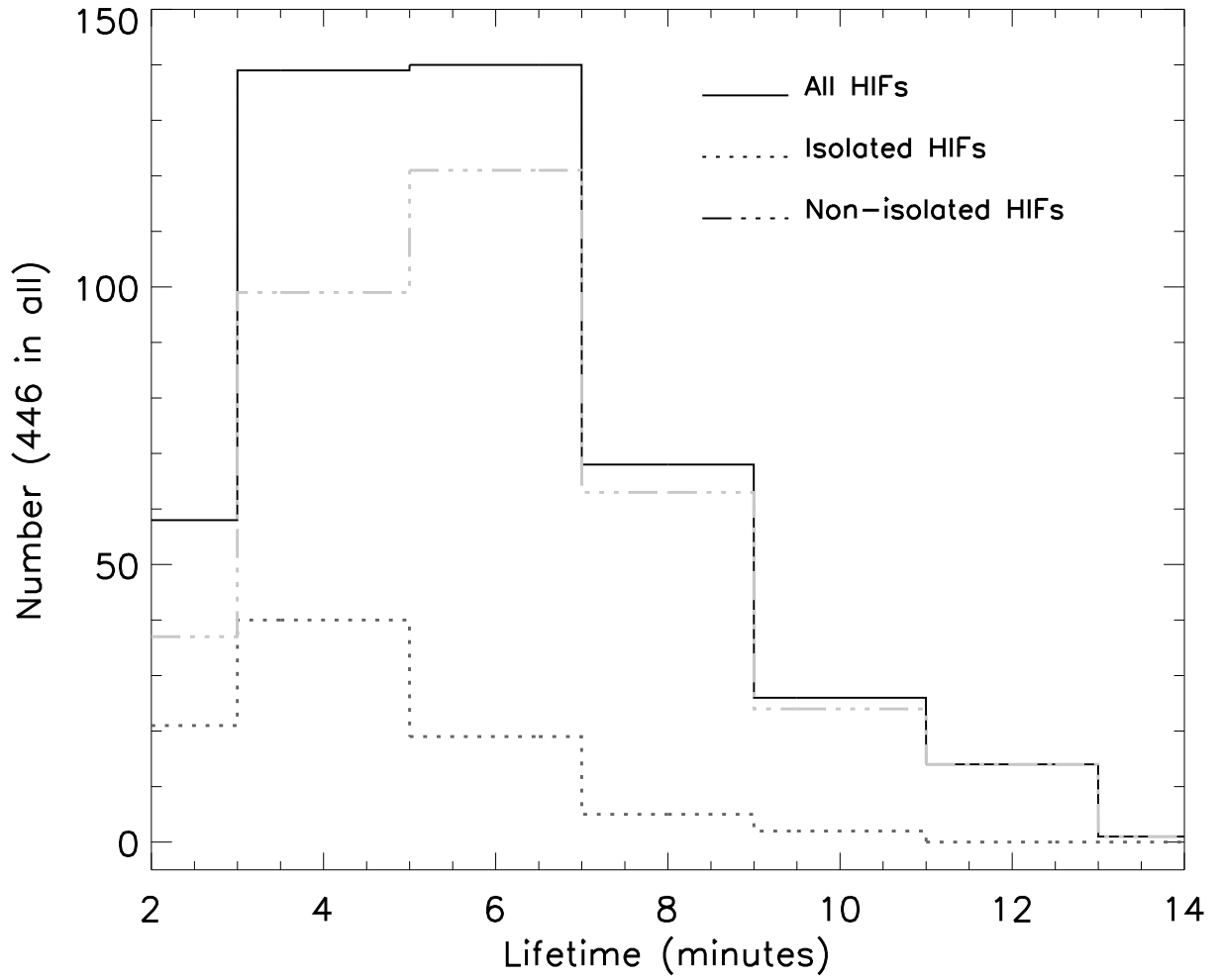


Fig. 4.— Histogram showing the distributions of lifetime for HIFs. The dotted line displays the histogram for isolated HIFs, the dash-dot-dot line for non-isolated HIFs, and the solid line for all HIFs.

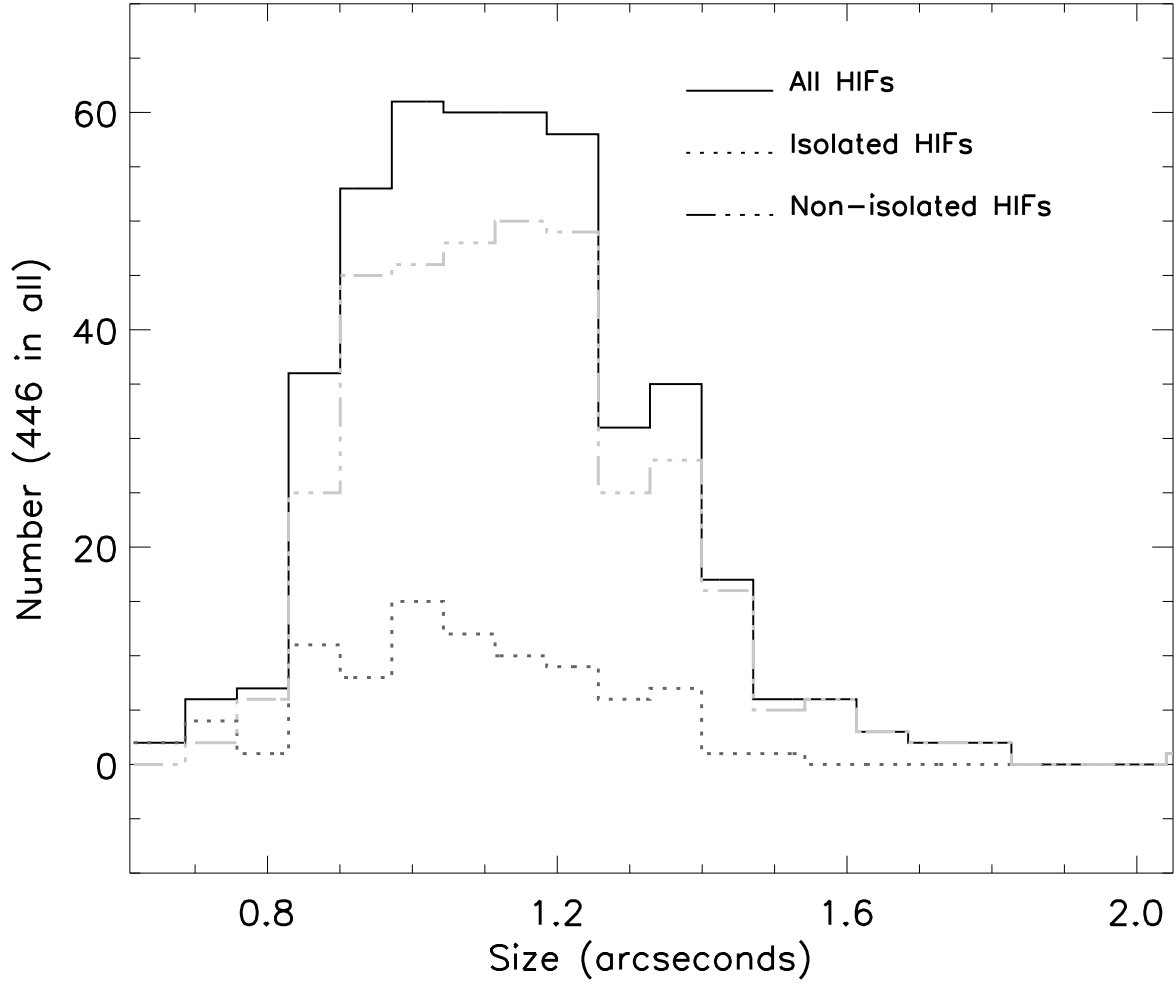


Fig. 5.— Similar to Fig. 4, but for the histogram of size of HIFs.

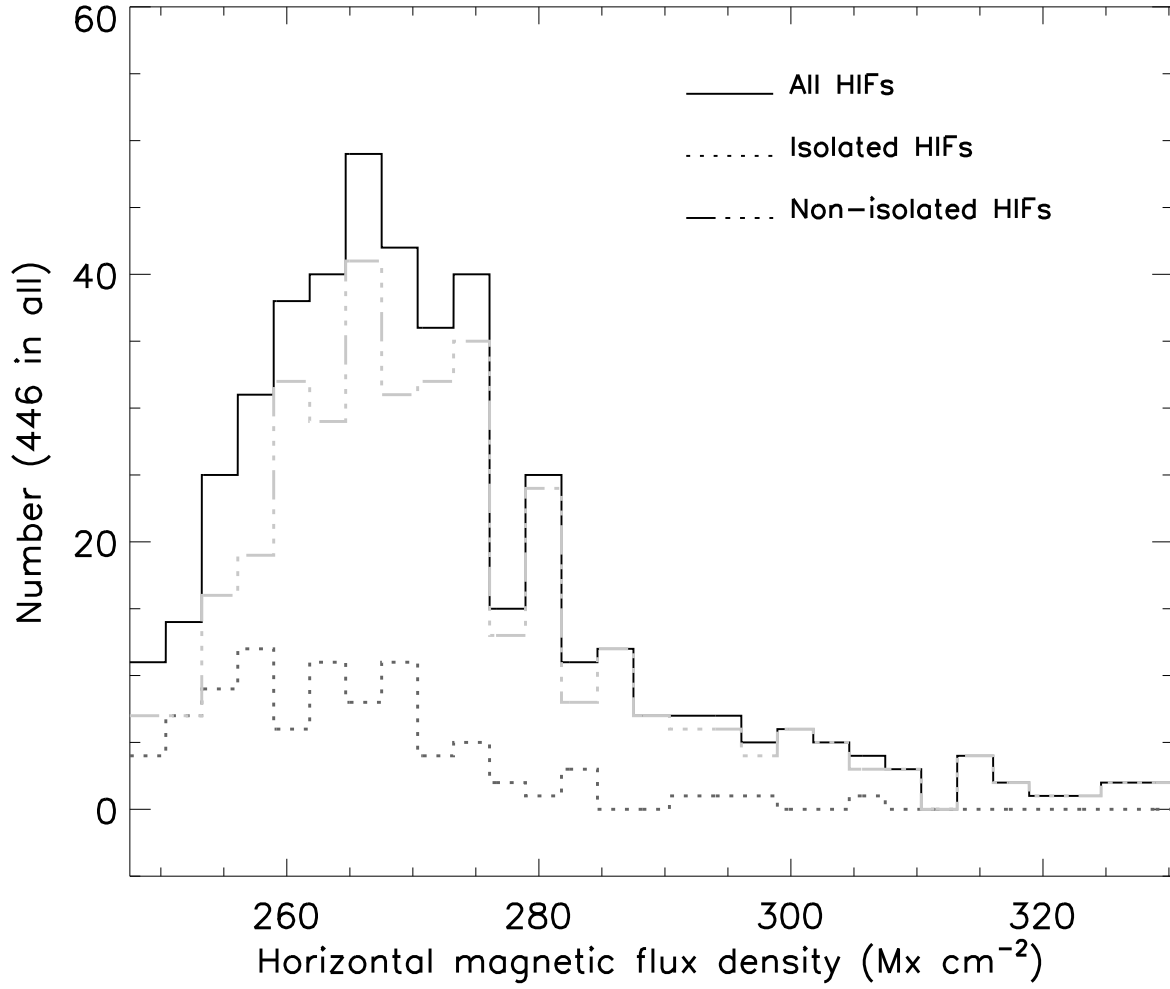


Fig. 6.— Similar to Fig. 4, but for the histogram of horizontal magnetic flux density of HIFs.

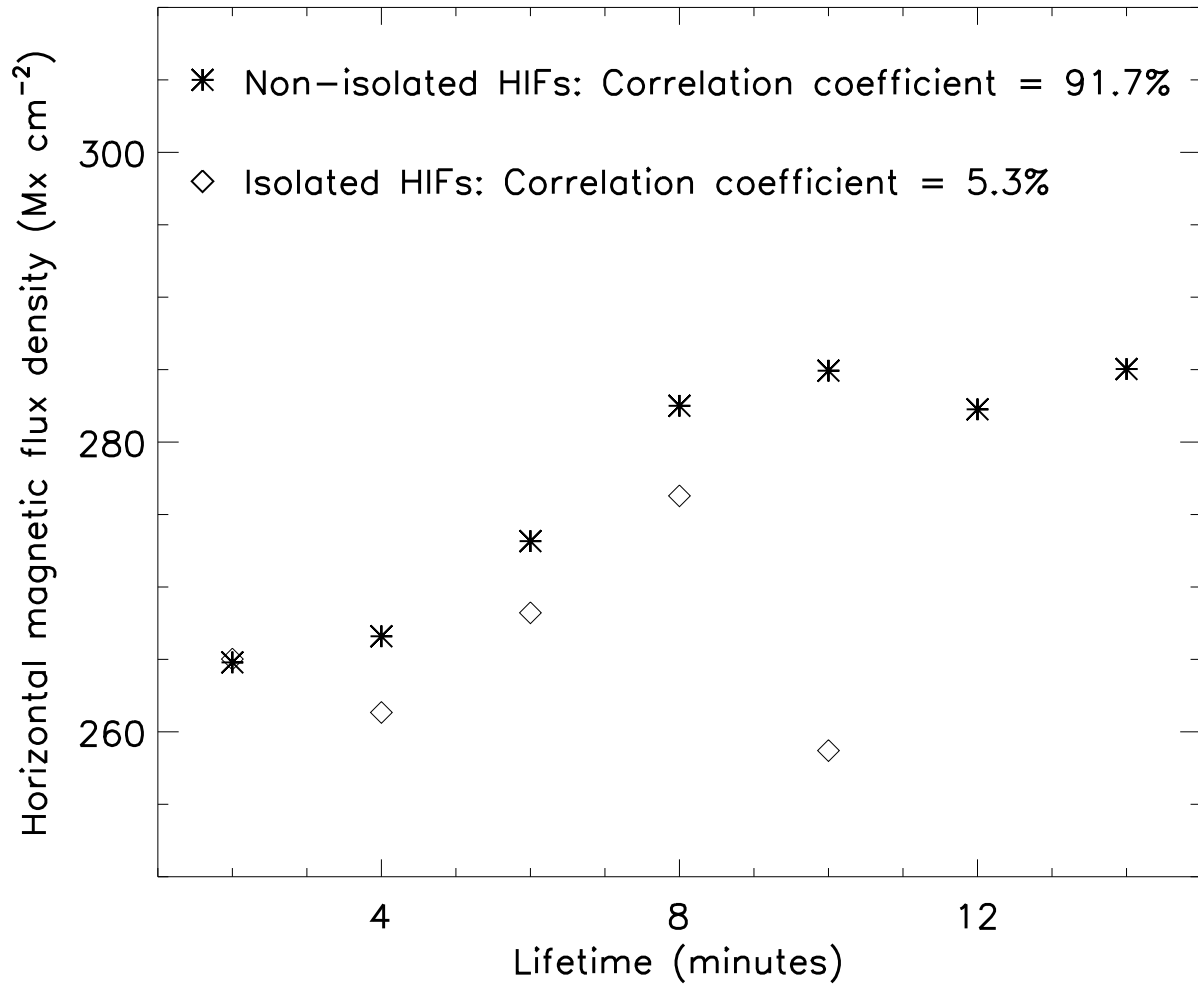


Fig. 7.— Relationship between lifetime and horizontal magnetic flux density of HIFs. The asterisks mean the properties of non-isolated HIFs, and the diamonds show the one of isolated HIFs.

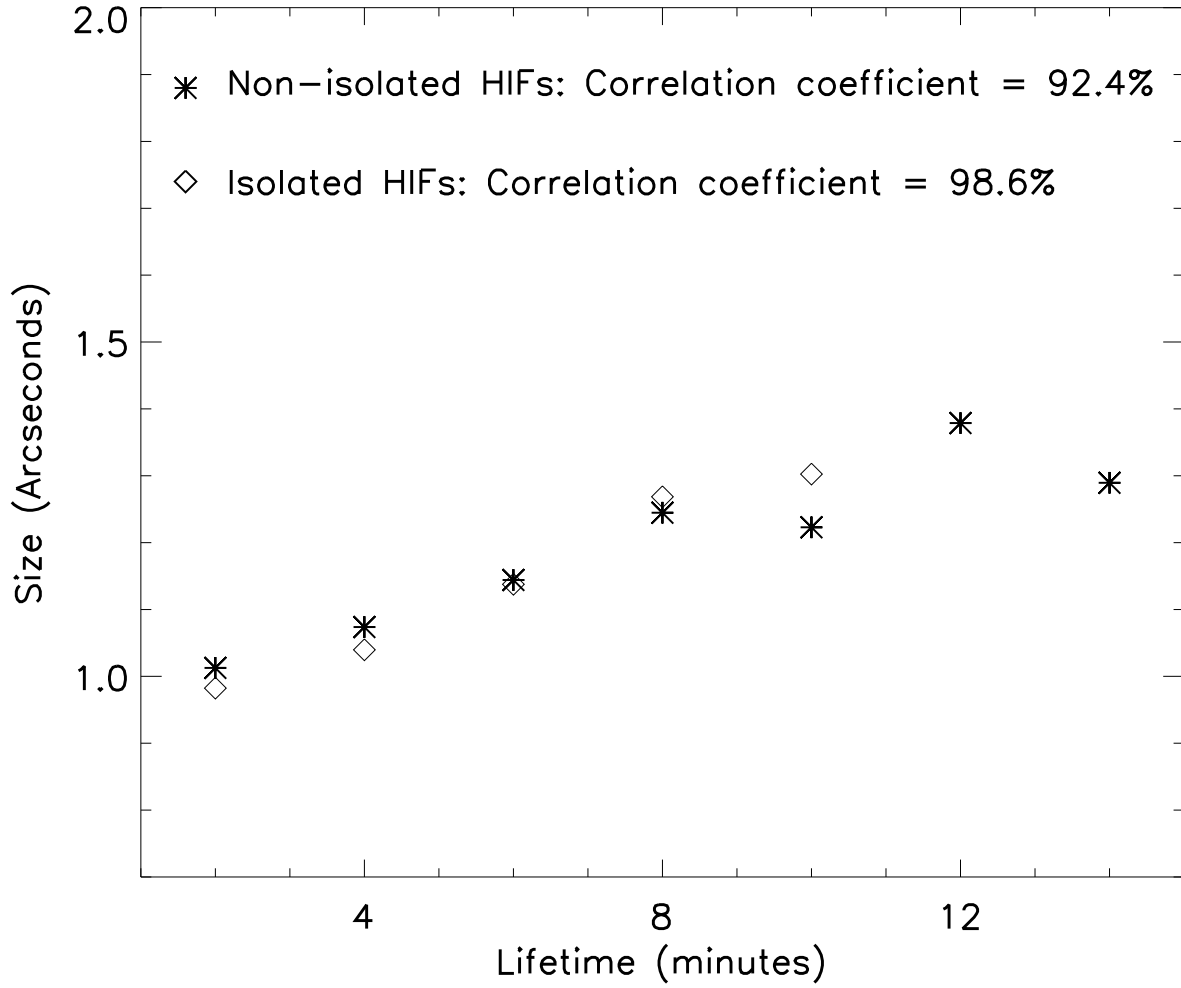


Fig. 8.— Relationship between lifetime and size of HIFs. The asterisks mean the properties of non-isolated HIFs, and the diamonds show the one of isolated HIFs.

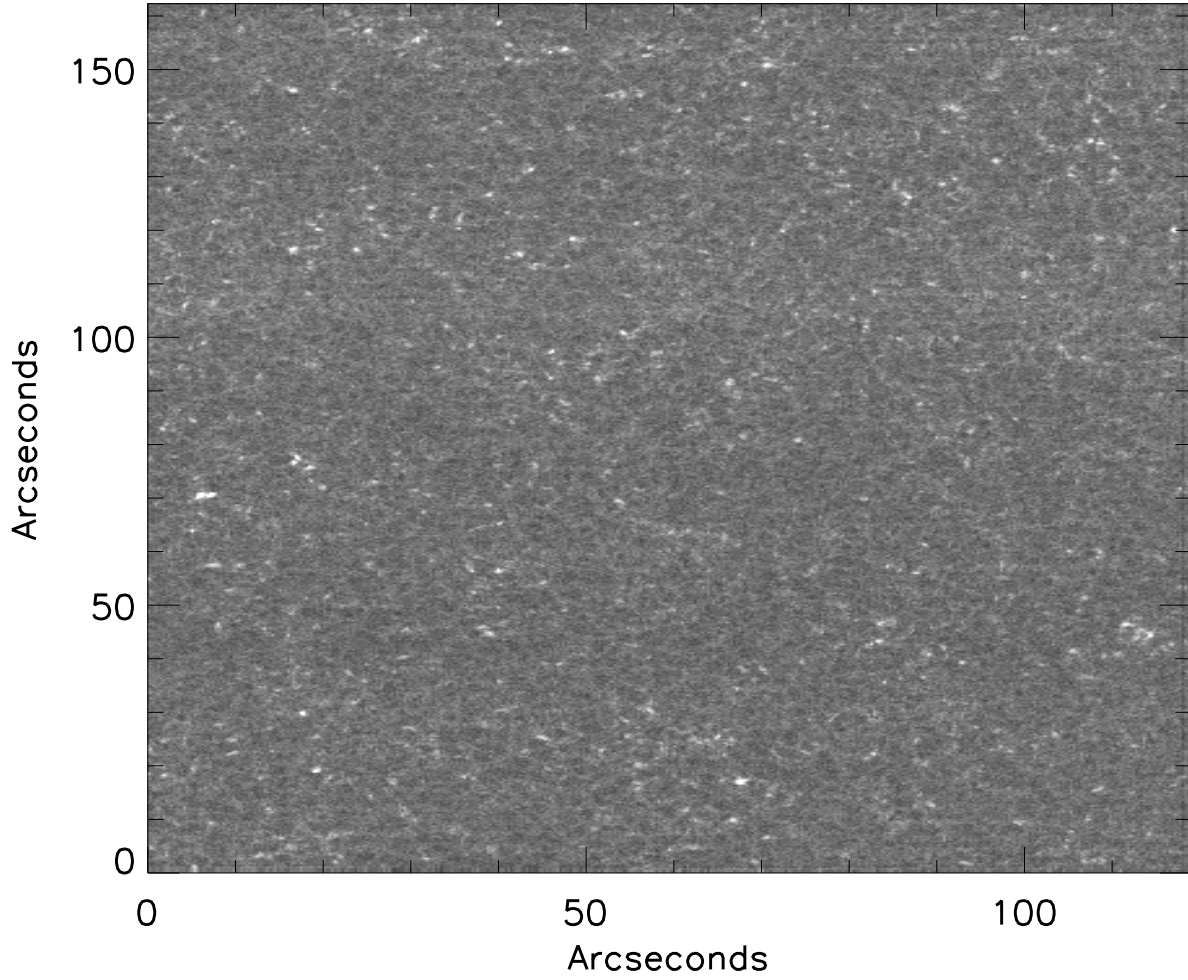


Fig. 9.— Distributions of horizontal magnetic flux density for quiet region observed on 2007 May 11. The gray scale saturates at $0.0025 I_c$ for linear polarization degree.

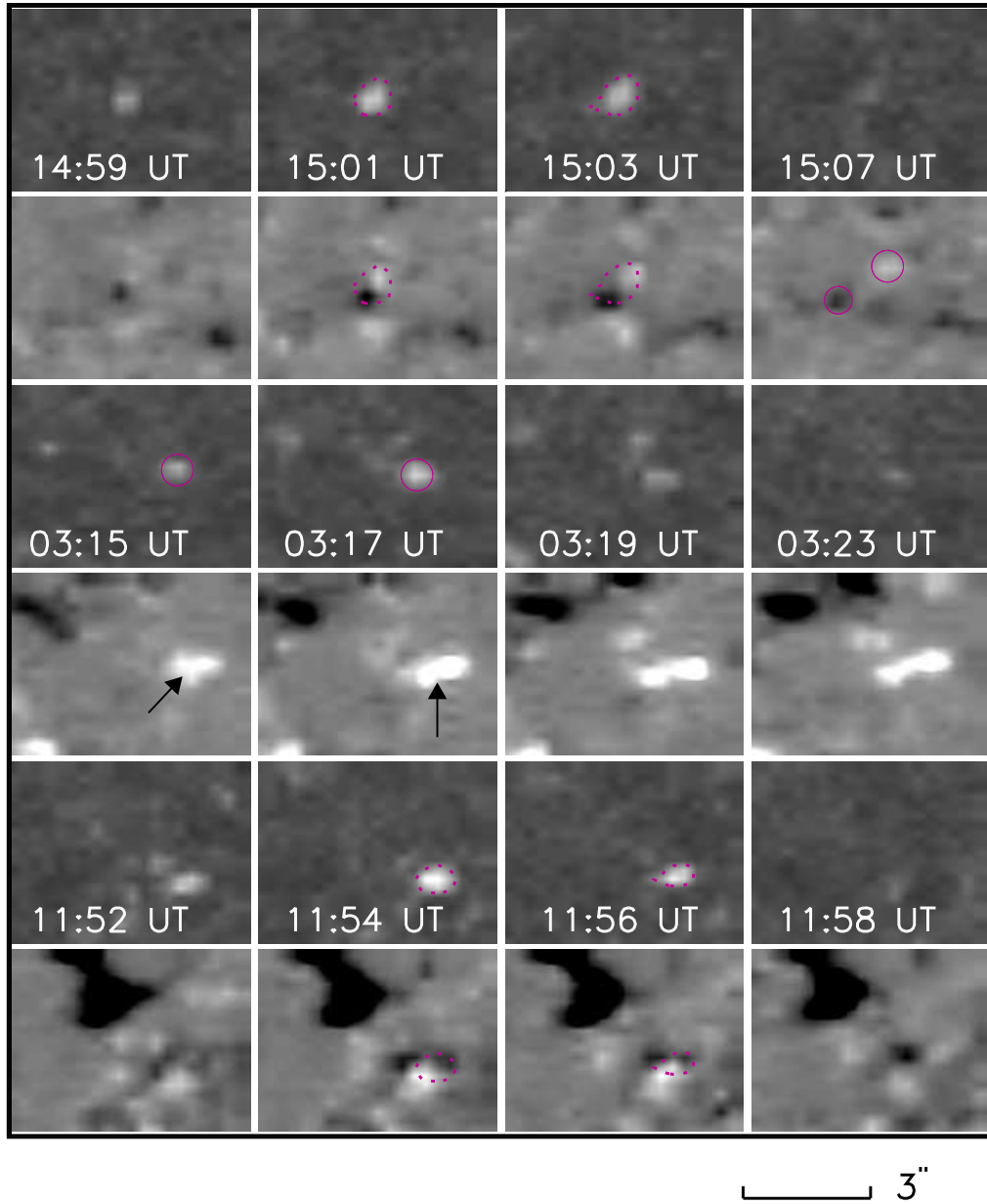


Fig. 10.— Example for non-isolated HIFs. The first line displays the horizontal magnetic elements observed on 2007 June 1, and the second one denotes the corresponding vertical magnetic elements. This is a typical case of magnetic topology configurations for Ω loop. The polarization signals in the third and fourth lines, observed on 2007 April 13, exhibit the example of only one footpoint in side of the region of linear polarization signal. The magnetic elements in the fifth and sixth lines, observed on 2007 June 2, reveal the example of undistinguishable magnetic configuration. The bar in the low right corner represents the scale of 3''.